Formation of an Air-Water Two-Phase Flow

PIERRE M. ADLER

Laboratoire de Mécanique
Expérimentale des Fluides
Bâtiment 502
Campus Universitaire, 91405
Orsay, France

The geometrical parameters of injection devices are shown to have almost no effect on the resulting two-phase flow, while they influence the pressure drop owing to its formation. The predominant hydrodynamic parameter is the ratio of the mean superficial velocities. A simplified analysis leads to good agreement with experimental results. The different causes of pressure drops are quantified.

SCOPE

A two-component, two-phase flow is obtained with a device in which the two phases are mixed. A particular kind of injection device has been studied. The air is introduced from air chambers through the wall of the mixing section into the flowing water. The mixing section is either constant or increasing downstream (referred to below as types I and II).

From a practical standpoint, it is useful to know how such a device works to evaluate the effect of the design, that is, of the geometrical parameters on the resulting flow just downstream, to determine the predominant hydrodynamic parameters, and to quantify the different causes of pressure drops.

Furthermore, since a separated flow model must be used to describe the formation of the mixture, expressions for interaction terms between phases can be tested by comparison with experimental data.

CONCLUSIONS AND SIGNIFICANCE

Data show that the two types of injection devices work quite differently. With type I, air passes from the air chambers into the flowing water mainly at the downstream end of the injection device; with type II, this occurs along the entire length of the device. In both cases, within the so-called mixing zone, downstream from the injection device, bubbles migrate towards the central part of the channel, and the flow quickly reaches a quasi stable state.

The predominant hydrodynamic parameter is the ratio of mean superficial velocities.

Geometrical parameters do not seem to have a significant influence on the resulting flow. However, when type II is used, the flow appears to be very sensitive to the geometrical defects of the assembly. The pressure drop due to the formation of the flow depends on the type of injection device, and for type II it depends on the geometrical parameters of the grids.

Interaction terms between phases were phenomenologically deduced. A model was then derived and compared with experimental data. Agreement was good. Three causes of pressure losses were quantified: friction loss within the injection device, acceleration, and friction pressure drop within the mixing zone.

Finally, the choice of type I or II depends on what is needed. In order to obtain a well-defined flow, type I must be selected. If pressure drop must be minimized, type II is preferable.

Many different types of injection devices were studied, but, as they have been completely reviewed (Adler, 1975), only the main ones are described below.

1. Air is introduced from an air chamber into the liquid flow through several holes at the tube wall (Oya, 1971) or through staggered porous tubes spanning the cross section (Muir, 1963).
2. Liquid-gas ejectors, in which the liquid serves as the driving medium entraining the gas, were used by Witte (1965) and Deich (1971).
3. Air is introduced through the porous wall of the mixing section into the flowing water (Delhaye, 1970; Smith et al., 1968; Wallis, 1961); the mixing section is either constant or increases downstream.

This third type of injection device was selected for this study, as it can be easily described by few geometrical parameters. Sekoguchi et al. (1968) and Yip et al. (1970) partially studied the influence of these parameters for type 1, but no systematic study has been made, to our knowledge, for type 3.

Another kind of study should also be recalled (Hewitt and Hall-Taylor, 1970; Hutchinson et al., 1973; Whalley et al., 1974); these authors studied the influence of upstream boundary conditions, when the liquid phase was introduced into an air stream either through a porous wall or by a central nozzle. Experimental and theoretical analyses led to the conclusion that the initial liquid distribution has a significant influence on the flow except far downstream.

In this paper, injection devices of type 3 with a constant or an increasing cross section (referred to below as types I and II)are investigated for horizontal air-water flow. Following a brief description of the experimental facility

P. Adler is at Laboratoire de Biorhéologie et d'Hydrodynamique Physiologique, Tour 33/34, 2ème étage, 2 Place Jussieu, 75221 PARIS CEDEX 05, France.

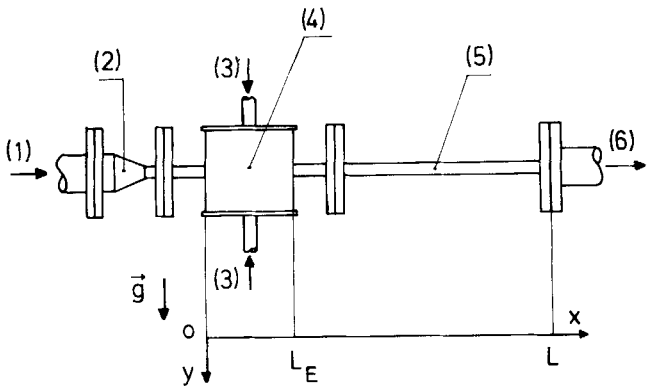

Fig. 1. Schematic diagram of apparatus: (1) water inlet, (2) convergent, (3) air inlet, (4) injection device, (5) channel of rectangular cross section (24 × 120 mm²), (6) outlet.

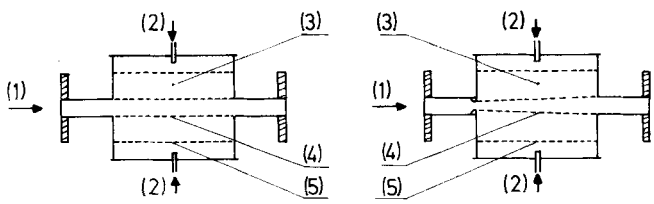

a. constant section b. increasing section

Fig. 2. Schematic diagram of injection devices: (1) water inlet, (2) air inlet, (3) air chamber, (4) perforated plate, (5) diffusor.

and of measurements, the data are presented and discussed and the predominant parameters determined. A phenomenological form is proposed for the interaction terms between phases. Applied to the mixing zone, the subsequent analysis leads to good agreement with experimental results obtained with type I; the comparison is less favorable with type II.

EXPERIMENTAL APPARATUS AND MEASUREMENTS

The apparatus, schematically drawn in Figure 1, is composed of a converging channel, the injection device, and a channel of rectangular cross section 24 × 120 mm².

The injection devices (Figure 2) are made up of two rectangular perforated plates (120 mm × L_E) through which air at equal flow rates is introduced into the water; circular holes of diameter d are arranged in a hexagonal pattern in these plates (which can be replaced by porous plates). Two intermediate perforated plates are provided to diffuse the air.

The injection devices of type I have a rectangular cross section 24 × 120 mm². The upstream and downstream sections of the injection devices of type II are always 12 × 120 and 24 × 120 mm², respectively.

A rectangular cross section was chosen to provide translational symmetry along the z axis, which respects the symmetry induced by gravity. Hence, with this geometry, it may be expected that the flow in the central part of the channel does not depend on z. Thus local void fraction measurements in the vertical symmetry plane of the apparatus will be well representative of the flow.

The following set of parameters (Adler, 1975), deduced from a similarity analysis (assuming no transfer between phases, isothermal flow, constant physical properties), is expressed as

water inlet conditions
geometric parameters:

$$\frac{L_E}{D_H}, \frac{d}{D_H}, \frac{S_1}{S_2}, \frac{D_E}{D_H}, \frac{L}{D_H}$$

Table 1. Experimental Parameters

S_1/S_2	1-0.5
d, mm	Porous-0.8-3
L_E, mm	100-200
$\overline{U}_G$, m/s	4.26-5.11-5.96
$\overline{U}_L$, m/s	2.12-2.89-3.66

hydrodynamic parameters:

$$\frac{\rho_L \overline{U}_L D_H}{\mu_L}, \frac{\overline{U}_G}{\overline{U}_L}, \frac{\overline{U}_L}{\sqrt{g D_H}}, \frac{\sigma}{\rho_L \overline{U}_L^2 D_H}, \frac{\mu_G}{\mu_L}, \frac{\rho_G}{\rho_L},$$

For each type of injection device, six geometric arrangements were studied. For each arrangement, nine flow conditions were tested as summarized in Table I.

Air and water flow rates are measured, respectively, with two sonic throats and a turbine flowmeter; mass flow rates are constant.

Pressure taps are horizontal to avoid errors induced by gravity. Pressures are measured with strain gauges. Each data point is the mean of five measurements.

The local void fraction is measured with a variable impedance probe (Lecroart and Porte, 1971). Briefly, the probe consists of a cylindrical metal tube housing a thin tungsten wire (diameter and length about 10 and 30 μm, respectively), insulated except at the tips. The impedance variations between the wire and the tube are converted into electrical signals.

RESULTS AND DISCUSSION

The formation of the two-phase flow is briefly described, using pressure and local void fraction measurements. Predominant hydrodynamic and geometric parameters are determined.

Description of the formation of the air-water flow

Injection devices with constant section. From the overall rough pressure measurements given in Figure 3, it may be concluded that four regions are distinguishable.

A constant pressure region occupies the major portion

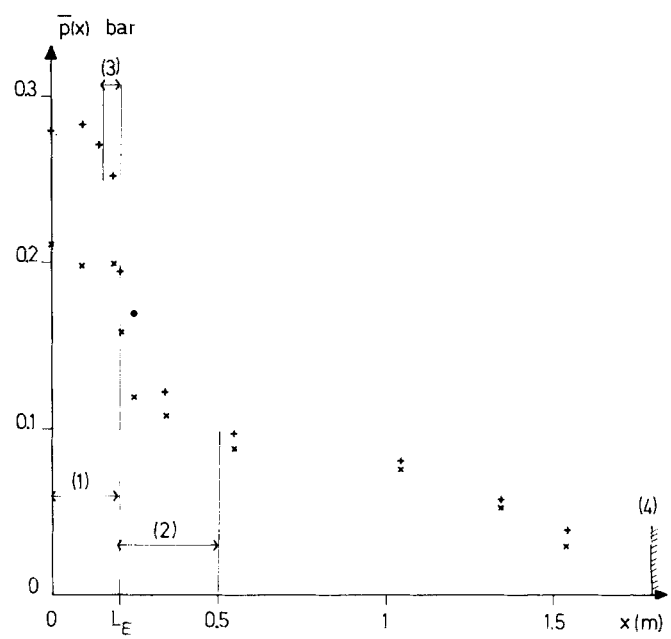

Fig. 3. Relative pressure as a function of the horizontal coordinate x for type I (+; d = 0.8 mm) and type II (×; d = 3 mm). Common conditions: L_E = 200 mm, $\overline{U}_L$ = 2.89 m/s, $\overline{U}_G$ = 5.96 m/s). (1) extent of the injection device, (2) mixing zone, (3) injection zone for type I, (4) outlet.

of the injection device. This is due to the two air chambers, as pressure drop through the grids is very small. Moreover, the void fraction is very small in this region (Figure 4*a*; $x = 6.2$ cm); thus only a small air flow rate is introduced into the flowing water. In fact, the greatest fraction of the air flow rate (maintained constant by the sonic throats) is introduced through the downstream part of the grids in the so-called injection zone. In the channel, the air introduced is confined near the wall, owing to the fact that inertial air forces are weak.

At the end of the injection device, this very unstable pattern is quickly destroyed, and the two phases begin to mix within the channel. This is the mixing zone. The air migrates towards the central part of the channel, while the void fraction increases sharply (Figure 4*a*; $x = 12.3$ cm, 18.4 cm). The water is thus accelerated, and pressure decreases. Since vertical void fraction profiles are symmetrical, it is concluded that gravity effects are negligible in the mixing zone; it is shown below that inertial forces are predominant.

Downstream from the mixing zone, that is, at about $x = 55$ cm, flow reaches a quasistable state symbolized by the ∩ form of void fraction profiles (Figure 5*a*).

Injection devices with increasing section. Three flow zones were distinguished in the test section as revealed by overall pressure measurements (Figure 3).

The downstream part of injection device is roughly maintained at constant pressure, for the same reason as above. Thus, the water is not accelerated, and the air confined near the grids (Figure 4*b*; $x = 6.3$ cm) approximately fills the void owing to the enlargement of the cross section. Hence, in accordance with the value of the ratio S_1/S_2, the mean void fraction is about 0.5 at $x = L_E$.

Further on, in the so-called mixing zone downstream from the injection device, air migrates towards the central part of the channel (Figure 4*b*; $x = 12.3$ cm, 18.5 cm). The flow finally reaches a quasistable state symbolized by the ∩ form of void fraction profiles (Figure 5*b*). It should

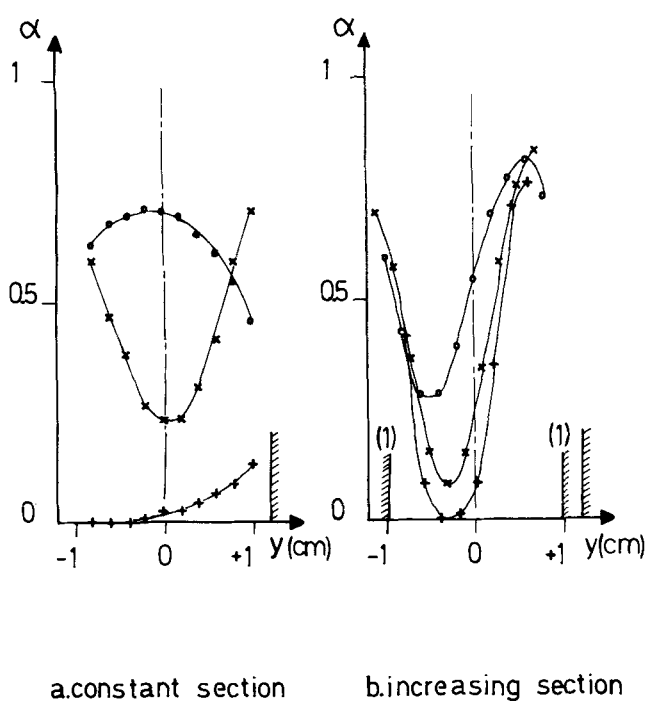

Fig. 4. Void fraction vs. vertical coordinate y for different values of the horizontal coordinate x within the injection device ($x = 6.2$ cm, +) and the mixing zone ($x = 12.3$ cm, ×; $x = 18.4$ cm, ○). Conditions: $\bar{U}_L = 2.12$ m/s, $\bar{U}_G = 4.26$ m/s, $L_E = 10$ cm, $d = 3$ mm. (1): upper and lower grids for $x = 6.2$ cm.

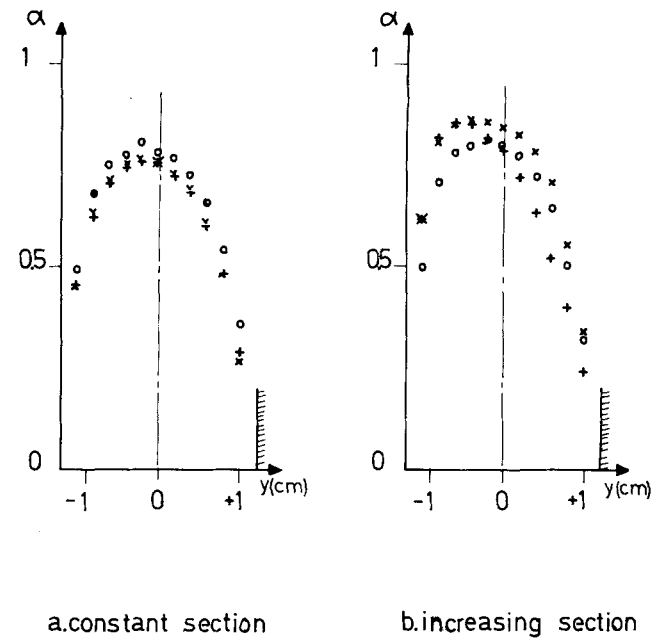

Fig. 5. Influence of geometric parameters on vertical void fraction profiles downstream from the mixing zone ($x = 55$ cm). Porous, $L_E = 10$ cm, +; porous, $L_E = 20$ cm, ×; $d = 0.3$ cm, $L_E = 20$ cm, ○. Flow conditions: $\bar{U}_L = 2.89$ m/s, $\bar{U}_G = 6.48$ m/s.

be noted that gravity forces are important within the test section since vertical void fraction profiles are asymmetrical (Figures 4*b* and 5*b*).

Comparison between the two types of injection device.

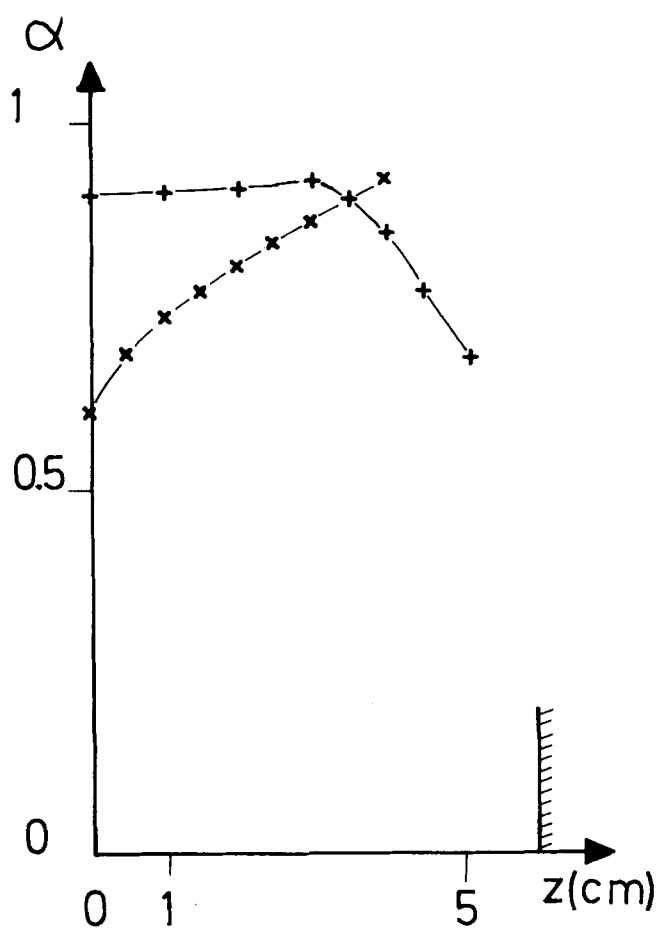

Fig. 6. Local void fraction as a function of the horizontal transversal coordinate z downstream from the mixing zone ($x = 55$ cm). Data are for type I(+), type II(×).

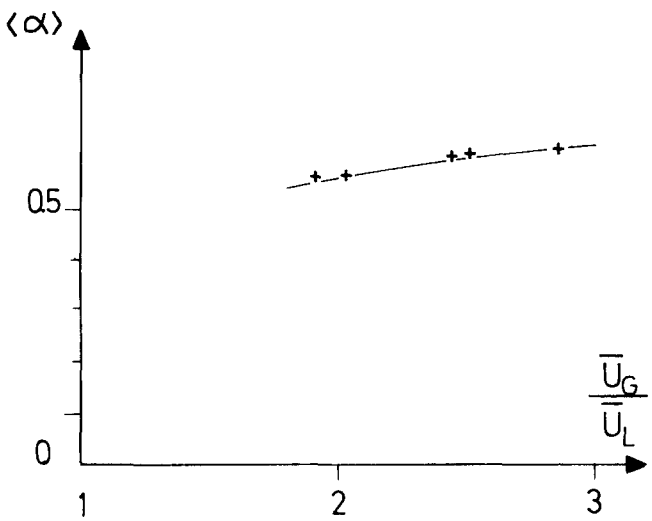

Fig. 7. Mean void fraction as a function of the ratio of mean superficial velocities downstream from the mixing zone ($x = 55$ cm). Data(+) are for: type I, porous grids, $L_E = 20$ cm. Solid line is prediction of Hughmark's formula.

Some significant differences between types I and II should be pointed out.

To start with, they work quite differently. With type I, air is mainly introduced into the flowing water at the downstream end of the injection device, and the void fraction is very low at $x = L_E$. With type II, it is introduced through the entire length of the grids, and the mean void fraction is about 0.5 at $x = L_E$. Hence, the acceleration pressure drop within the mixing zone, where the void fraction varies toward its equilibrium value, is much higher when type I is used; this is clearly seen on Figure 3.

Finally, when the flow reaches its quasiequilibrium state, it does not depend on z in the central part of the channel when type I is used (Figure 6), whereas it does with type II. Since the translational symmetry along the z axis respects gravity, this asymmetrical character of horizontal void fraction profiles can only be due to the sensitivity of the flow to geometric defects of the system. Consequently,

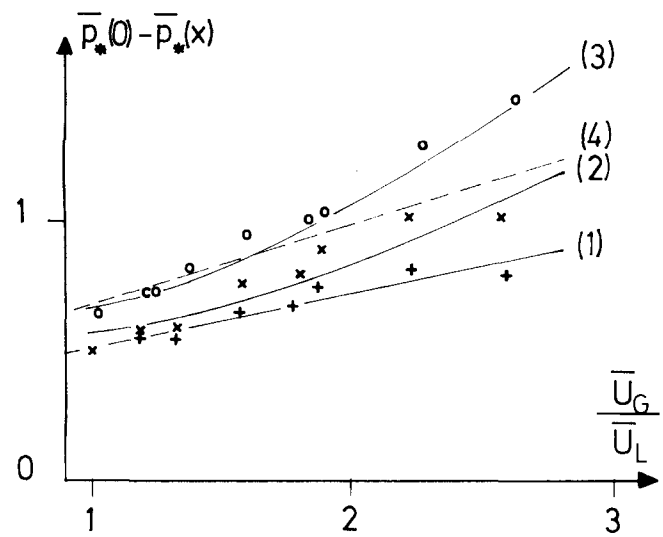

Fig. 9. Nondimensional pressure drop for type II within the mixing zone as a function of the ratio of the mean superficial velocities. Data ($x = 21$ cm, +; $x = 25$ cm, ×; $x = 35$ cm, ○) are for: porous grids, $L_E = 20$ cm. Solid lines: (1) regression line at $x = 21$ cm, (2) and (3) are deduced from the model at $x = 25$ cm and $x = 35$ cm. Broken line (4): regression line at $x = 21$ cm for $d = 3$ mm.

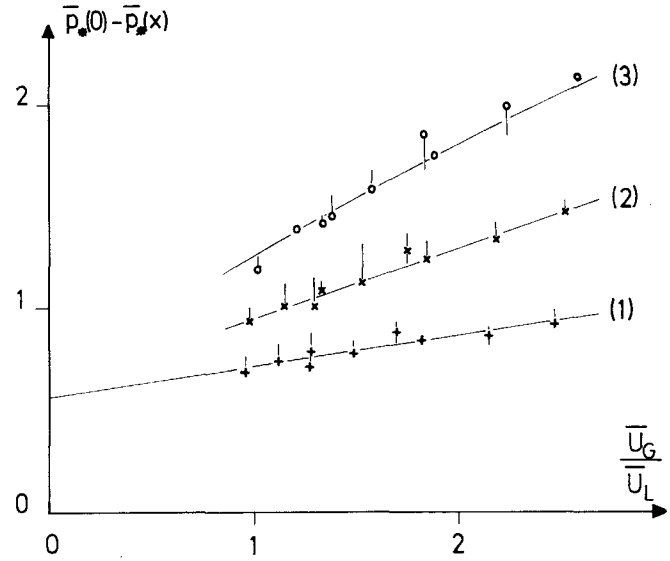

Fig. 8. Nondimensional pressure drop for type I within the mixing zone as a function of the ratio of the mean superficial velocities. Data ($x = 21$ cm, +; $x = 25$ cm, ×; $x = 35$ cm, ○) are for porous grids, $L_E = 20$ cm. Vertical bars represent the pressure drop range when the diameter d is varied. Solid lines: (1) regression line given by Equation (9), (2) and (3) are deduced from the model.

vertical void fraction profiles can only be used quantitatively when they are obtained with type I.

Influence of Hydrodynamic Parameters

The influence of hydrodynamic parameters is examined on mean void fraction of the resulting flow and on pressure drops due to the formation of the two-phase flow.

For horizontal slug or bubble flow, when it is fully established (Hughmark, 1962, 1965), the slip ratio Γ is given by

$$\Gamma = 1.2 + 0.2 \cdot \frac{\overline{U}_G}{\overline{U}_L} \tag{1}$$

Thus, mean void fraction only depends on the ratio $\overline{U}_G/\overline{U}_L$, as clearly confirmed by the data relative to type I, when flow reaches the quasistable state at about $x = 55$ cm (Figure 7). Moreover, Equation (1) agrees well with the data, though the flow is not yet fully established.

It should be emphasized that the flow is bubbly throughout the mixing zone and at $x = 55$ cm, though the overall flow conditions correspond to a slug pattern (Mandhane et al., 1974). This is due to the fact that the flow is not yet fully established.

As previously mentioned, a comparison of (1) with data obtained with type II is not made, since void fraction depends on z.

Pressure drops between $x = 0$ and the mixing zone are nondimensionalized by $\rho_L \overline{U}_L^2$ and represented as functions of the ratio $\overline{U}_G/\overline{U}_L$.

For type I, it is clearly shown that $\overline{U}_G/\overline{U}_L$ is the predominant hydrodynamic parameter (Figure 8). This is consistent with a rough application of the two-phase momentum equation. When the void fraction varies from 0 to an equilibrium value given by $\overline{U}_G/(\overline{U}_L + \Gamma\overline{U}_L)$, the acceleration pressure drop is expressed as

$$\frac{\Delta \overline{p}}{\rho_L \overline{U}_L^2} = \frac{\overline{U}_G}{\Gamma \overline{U}_L} \tag{2}$$

Hence it depends only on $\overline{U}_G/\overline{U}_L$.

Similar data obtained with type II are not so well correlated (Figure 9). This seems to derive from the fact that

the acceleration drop is not so predominant, since the void fraction only varies from 0.5 to the equilibrium value. A supplementary parameter could surely be introduced to describe the data, but this was not attempted owing to the limited amount of data.

Influence of geometric parameters

In order to simplify the discussion, each type of injection device is studied separately with variations in the geometric parameters L_E/D_H and d/D_H. The two types of injection devices are compared, that is, the ratio S_1/S_2 is altered. Only some results are given here; complete data can be found in Adler (1975).

Injection device with constant section. Since flow does not depend on z in the central part of the channel, vertical void fraction profiles can be meaningfully compared in order to indicate the influence of geometric parameters on the resulting flow. At $x = 55$ cm, this influence, if any, is seen to be very weak (Figure 5*a*). Thus the flow field is already independent of the geometric parameters very near the end of the injection device.

Moreover, geometric parameters have only a slight influence on pressure drop within the mixing zone (indicated by bars in Figure 8).

Injection device with increasing section. Vertical void fraction profiles at $x = 55$ cm do not differ significantly (Figure 5*b*), but no final conclusion can be drawn about the influence of geometric parameters. Pressure drops within the mixing zone are more clearly influenced by these parameters, as illustrated by an example in Figure 9.

Influence of the type of injection device. No decisive conclusion can be drawn from the comparison of Figures 5*a* and *b*. However, it can be stated that the resulting flow is much better defined when type I is used, since the flow does not depend on z.

As noted previously, it is clear that the pressure drop due to the formation of two-phase flow is smaller when type II is used (Figures 8 and 9). This pressure drop will be quantified after the analysis of the mixing zone.

ANALYSIS OF THE MIXING ZONE

One of the main unsolved problems in two-phase flow analysis is the expression of the interaction terms between phases. General but untractable forms for these terms have been known for a long time (Vernier and Delhaye, 1968), and some expressions are available (Zuber, 1964; Yaron and Galor, 1973). Furthermore, they must include a differential part (Bouré, 1973; Réocreux, 1974), as explained below.

A separated flow model is proposed. The main assumptions are given and discussed below, while detailed equations are to be found in the appendix. Local equations are spatially averaged. The analysis, restricted to one-dimensional flow, is thus approximate in character. The resulting system is derived and numerically integrated when boundary conditions are given. Experimental and calculated pressure drops are compared.

It should be noticed that the model was primarily derived for comparison with the data obtained with type I.

Interaction terms

Two forces are usually considered to be applied on a single sphere in an infinite liquid medium: drag proportional to

$$\rho_L \cdot (v_G - v_L)^2 \cdot \pi r^2 \tag{3}$$

and virtual mass force given by

$$-\frac{\rho_L}{2} \cdot \frac{4}{3} \cdot \pi r^3 \cdot \frac{D(v_G - v_L)}{Dt} \tag{4}$$

Instead of considering a spherical bubble moving in a liquid sphere (Zuber, 1964; Yaron and Galor, 1973), the bubble is assumed to move in a mixture of approximate density $\rho_L(1-\alpha)$. Hence, the virtual mass force is modified as

$$-\frac{\rho_L}{2} \cdot (1-\alpha) \cdot \frac{4}{3} \cdot \pi r^3 \cdot \frac{D(v_G - v_L)}{Dt} \tag{5}$$

which is a differential interaction term.

The drag is now assumed to be proportional to

$$-\rho_L \cdot (1-\alpha) \cdot f(v_G, v_L) \cdot \pi r^2 \tag{6}$$

where $f(v_G, v_L)$ will be given later.

Derivation of the system

A first set of assumptions must be expressed in order to derive the local equation system:

I
- Steady state flow.
- Gravity, viscous, and inertial forces of the gas phase, interfacial tension, mass transfer between phases are neglected.
- Constant physical properties.

The gas density is considered as a constant, since pressure drop in the mixing zone is small.

The system of local equations is detailed in the appendix as I. Interaction terms appear in the gas momentum equation. The symbol $\hat{r}$ must not be confused with the real radius of the bubbles. It is a characteristic length of the two-phase flow, proportional to some mean radius of bubbles, but the proportionality coefficient is unknown.

This system is then averaged over the cross section of the channel (system II in the appendix). A second set of assumptions must be made to get a tractable system:

II
- Temporal and spatial correlation coefficients are all equated to 1.
- Transverse velocities are neglected.
- If Γ is the slip ratio given by (1), then

$$-\frac{\rho_L}{\hat{r}} \cdot \langle\langle\alpha\rangle\rangle \cdot (\bar{v}_{1G} - \Gamma \bar{v}_{1L})^2 = -\mu_L \cdot \left\langle\left\langle \frac{\partial^2}{\partial x_2^2} (\alpha_L \bar{v}_{1L}) \right\rangle\right\rangle - \frac{\rho_L}{\hat{r}} \cdot \langle\langle \alpha_L \bar{f}(v_G, v_L) \rangle\rangle \tag{7}$$

- The friction pressure drop is expressed as twice the classical pressure drop in fully established flow:

$$-\mu_L \cdot \left\langle\left\langle \frac{\partial^2}{\partial x_2^2} (\alpha_L \bar{v}_{1L}) \right\rangle\right\rangle = \frac{0.316\, \rho_L \overline{U}_L^2}{D_H \langle\langle\alpha_L\rangle\rangle^{1.75} \cdot \left(\frac{U_L D_H}{\nu_L}\right)^{0.25}} \tag{8}$$

The mean value of the interaction term $f(v_G, v_L)$ is so expressed by (7), that the equation has the same general features as (3), and that it vanishes when the flow is fully established.

Moreover, this is closely associated with the two-dimensional character of the flow, which was neglected everywhere else in the spatially averaged equations.

The assumption about friction losses is rather crude, but this is not the predominant term in the equations for injection devices of type I. The two last assumptions are contradictory, since the friction losses at equilibrium would be equal to twice the real value. This point does not really

matter, for the analysis is restricted to the mixing zone.

Introduction of nondimensional quantities and elimination of $\overline{v}_{1G}$ and $\overline{v}_{1L}$ lead to the system referred as III in the appendix. The predominant parameter in III is the ratio $\overline{U}_G/\overline{U}_L$.

Boundary conditions

Injection devices with constant section. Pressure results at $x = 21$ cm (Figure 8) are fitted by the regression line

$$p_*(0) - p_*(21\text{ cm}) = a \cdot \frac{\overline{U}_G}{\overline{U}_L} + b \qquad (9)$$

where a and b are equal to 0.14 and 0.6, respectively.

The friction pressure drop within the injection device cannot be closely dependent on the ratio $\overline{U}_G/\overline{U}_L$, since the void fraction is very small in the injection device. Hence this friction pressure drop will be assumed to be equal to b. Furthermore, the acceleration pressure drop between $x = 0$ and $x = 21$ cm is assumed to be equal to $a \cdot \overline{U}_G/\overline{U}_L$. Thus

$$\frac{<<\alpha>>\ (x = 21\text{ cm})}{1 - <<\alpha>>\ (x = 21\text{ cm})} = a \cdot \frac{\overline{U}_G}{\overline{U}_L} \qquad (10)$$

Hence $<<\alpha>>\ (x = 21$ cm) is readily deduced from (10), while initial conditions for pressure are given by (9).

Injection devices with increasing section. As previously seen from the data, the mean void fraction is approximately equal to 0.5 at $x = L_E$.

When the ratio $\overline{U}_G/\overline{U}_L$ is smaller than 1.5, the mean void fraction at $x = L_E$ is greater than its final value; water in such conditions is decelerated, but it is assumed that no negative acceleration pressure drop occurs; that is, the energy relative to this pressure drop is dissipated. The initial value for pressure is deduced from the regression line at $x = 21$ cm. For the sake of simplicity, the void fraction is actually equated to 0.5 at that point.

Comparison with experimental results

System III was numerically integrated using the Runge-Kutta-Gill method. The truncation error was found to be negligible. $\hat{r}$ was obtained by fitting theoretical and experimental results relative to type I with porous grids and was found to have a value of 5 cm. For type I, good agreement between the model and the data was obtained (Figure 8). It was thus concluded that the model leads to essentially correct results.

The model was then directly applied to type II, though the physical situation is quite different; inertial forces are not as predominant as for type I, since water is only weakly accelerated. Thus, friction losses and gravity effects are important. It would be difficult to really modify the model without taking into account the three-dimensional character of the flow. But this approximate analysis still shows good agreement with experimental data of type II when porous grids are used (Figure 9). However, detailed results (Adler, 1975) show that the comparison becomes steadily worse with increasing hole diameter.

Evaluation of pressure drop

A distinction between acceleration and friction pressure drops can be quantitatively derived from the above boundary conditions and from the model.

For injection devices with constant section, the total pressure drop caused by the formation of the two-phase flow is considered as the sum of three terms: a friction pressure drop originating in the injection device and approximately equal to $0.6\ \rho_L\overline{U}_L^2$ [as deduced from (9)]; an acceleration pressure drop within the mixing zone related to the variation of the void fraction from 0 to its equilibrium value $<<\alpha>>$, given by (2)

$$\frac{<<\alpha>>}{1 - <<\alpha>>} \cdot \rho_L\overline{U}_L^2$$

and a friction pressure loss in the mixing zone which can be neglected in the first step.

For injection devices with increasing section, the total pressure drop is evaluated as the sum of three terms:

1. The friction pressure drop within the injection device is about $0.8\ \rho_L\overline{U}_L^2$ minus the pressure recovery when $\overline{U}_G$ is equated to zero. Experimental evidence for this point is found in Adler (1975).

2. Two cases must be distinguished for the acceleration pressure drop in the mixing zone. When the limiting void fraction value is lower than 0.5, it is assumed that no negative pressure drop occurs owing to water deceleration. Conversely, as the mean void fraction is about 0.5 at $x = L_E$, the pressure drop is given by $\rho_L\overline{U}_L^2 \cdot \dfrac{2<<\alpha>> - 1}{1 - <<\alpha>>}$.

3. A friction loss within the mixing zone which can be neglected in a first step.

CONCLUSIONS

The significant phenomena have been investigated within the injection devices and the mixing zone.

The predominant hydrodynamic parameter is the ratio $\overline{U}_G/\overline{U}_L$.

Geometric parameters do not appear to have a decisive influence on the resulting two-phase flow. But the pressure drop due to formation of the flow depends on the type of the injection device and for type II depends on the geometric parameters of the grids.

A simplified analysis has been proposed to describe the evolution of void fraction and pressure within the mixing zone. Good agreement is obtained with data.

NOTATION

a, b = defined by (9)
D_E, D_H = hydraulic diameter of the injection device, of the channel
d = diameter of holes in plates
f = defined by (6)
g = acceleration of gravity
L, L_E = length of the system, of the grids
p = pressure
p_* = $\overline{p}/\rho_L\overline{U}_L^2$
$r, \hat{r}$ = radius and characteristic length of bubbles
S_1, S_2 = cross section of the injection device at $x = 0$, $x = L_E$
t = time
$\overline{U}_K$ = mean superficial velocity of phase K (given by the ratio of the volume flow rate of that phase and of the cross-sectional area of the channel)
$\vec{v}_K$ = velocity of phase K (components v_{ik})
x, y, z or x_1, x_2, x_3 = Cartesian coordinate system (Figure 1). The origin 0 is at the beginning of the injection device and within the intersection of the horizontal and vertical symmetry planes of the channel
α_K = probability of presence of phase K
Γ = slip ratio
μ_K, ν_K, ρ_K = dynamic viscosity, kinematic viscosity, density of phase K

σ = interfacial tension

Subscripts

K = phase K; $K = G$ (gas), $= L$ (liquid)

* = nondimensional quantity

Symbols

$< >, << >>$ = one-, two-dimensional spatial mean

$\overline{}$ = temporal mean

Δ = Laplacian

LITERATURE CITED

Adler, P., "Contribution à l'étude de la formation et de l'évolution d'une émulsion," Thèse de Doctorat es-Sciences Physiques, Université de Paris VI, Paris, France (1975).

Bouré, I. A., "Dynamique des écoulements diphasiques: propagation de petites perturbations," *Report n° R—4456*, Grenoble, France (1973).

Deich, M. Y., "A Method for Calculating a Two-Phase Jet Injector," *Heat Transfer. Sov. Res.*, 3 (1971).

Delhaye, J.-M., "Contribution à l'étude des écoulements diphasiques eau-air et eau-vapeur," Thèse de Doctorat es-Sciences Physiques, Université de Grenoble, Grenoble, France (1970).

Hewitt, G. F., and N. S. Hall-Taylor, *Annular Two-Phase Flow,"* Pergamon Press, New York (1970).

Hughmark, G. A., "Hold-Up in Gas-Liquid Flow," *Chem. Eng. Progr.*, **58**, 62 (1962).

———, "Hold-up and Heat Transfer in Horizontal Slug Gas-Liquid Flow," *Chem. Eng. Sci.*, **20**, 1007 (1965).

Hutchinson, P., et al., "Transient Flow Distribution in Annular Two-Phase Flow," Meeting American Nuclear Society on Reactor Heat Transfer, Karlsruhe (1973).

Lecroart, H., and R. Porte, "Electrical Probes for Study of Two-Phase Flow at High Velocity," International Symposium on Two-Phase System, Haifa, Israel, (1971).

Mandhane, I. M., et al., "A Flow Pattern Map for Gas-Liquid Flow in Horizontal Pipe," *Intern. J. Multiph. Flow*, **1**, 537 (1974).

Muir, J. F., and R. Eichhorn, "Compressible Flow of an Air-Water Mixture through a Vertical Two-Dimensional, Converging-Diverging Nozzle," *Proj Squid Tech. Rept, PR—105-P* (1963).

Oya, T., "Upward Liquid Flow in Small Tubes into Which Air Streams," *Bull., J.S.M.E.*, **14**, 1320 (1971).

Réocreux, M., "Contribution à l'étude des débits critiques en écoulements diphasiques eau-vapeur," Thèse de Doctorat es-Sciences Physiques, Université de Grenoble, Grenoble, France (1974).

Sekoguchi, K., et al., "The Influences of Mixers, Bends and Exit Sections on Horizontal Two-Phase Flow," Int. Symp. cocurrent gas-liquid flow, Waterloo (1968).

Smith, R. V., et al., "Two-Phase Two-Component Critical Flow in a Venturi," *AERE-R 5736* (1968).

Vernier, P., and J. M. Delhaye, "General Two-Phase Flow Equations Applied to the Thermohydrodynamics of Boiling Nuclear Reactors," *Energie Primaire*, **4** (1968).

Wallis, G. B., "Some Hydrodynamical Aspects of Two-Phase Flow and Boiling," International Heat Transfer Conference, Paper 38 (1961-62).

Whalley, P. B., et al., "Experimental Wave and Entrainment Measurements in Vertical Annular Two-Phase Flow," Symposium Multiphase Flow Syst., Glasgow, Scotland (1974).

Witte, J. H., "Efficiency and Design of Liquid Gas Ejectors," *Brit. Chem. Eng.*, **10**, 602 (1965).

Yaron, I., and B. Galor, "High Reynolds Number Fluid Dynamics and Heat and Mass Transfer in Real Concentrated Particulate Two-Phase Systems," *Intern. J. Heat Mass Transfer*, **16**, 887 (1973).

Yip, F. C., et al., "The Motion of Small Air Bubbles in Stagnant and Flowing Water," *Can. J. Chem. Eng.*, **48**, 229 (1970).

Zuber, N., "On the Dispersed Two-Phase Flow in the Laminar Flow Regime," *Chem. Eng. Sci.*, **19**, 897 (1964).

APPENDIX: THEORETICAL ANALYSIS OF THE MIXING ZONE

Under the assumptions I, the system of local equations is expressed as

I

continuity

$$\frac{\partial \alpha_K \overline{v}_{iK}}{\partial x_i} = 0$$

two-phase momentum

$$\frac{\partial}{\partial x_j}(\alpha_L \rho_L \overline{v_{iL} v_{jL}}) = -\frac{\partial \overline{p}}{\partial x_i} + \mu_L \cdot \Delta(\alpha_L \overline{v}_{iL})$$

gas momentum

$$0 = -\frac{\partial \overline{p}}{\partial x_i} - \rho_L \cdot \frac{(1-\alpha)}{\hat{r}} \cdot \overline{f}(v_G, v_L) - \rho_L \cdot \frac{(1-\alpha)}{2} \cdot \left(\overline{v_{jG} \cdot \frac{\partial v_{iG}}{\partial x_j}} - \overline{v_{jL} \cdot \frac{\partial v_{iL}}{\partial x_j}} \right)$$

The average system over the cross section of the channel is easily deduced from I as

II

$$<<\alpha \overline{v}_{1G}>> = \overline{U}_G$$

$$<<\alpha \overline{v}_{1L}>> = \overline{U}_L$$

$$\frac{d}{dx_1} <<\rho_L \alpha_L \overline{v_{1L}^2}>> - \mu_L \cdot \left\langle\left\langle \frac{\partial^2}{\partial x_2^2}(\alpha_L \overline{v}_{1L}) \right\rangle\right\rangle = -\frac{d}{dx_1} <<\overline{p}>>$$

$$0 = -\frac{d}{dx_1} <<\overline{p}>> - \frac{\rho_L}{\hat{r}} \cdot <<\alpha_L \overline{f}(v_G, v_L)>> - \frac{\rho_L}{2} \cdot \left\langle\left\langle \alpha_L \overline{v_{1G} \cdot \frac{\partial v_{1G}}{\partial x_1}} \right\rangle\right\rangle + \frac{\rho_L}{2} \cdot \frac{d}{dx_1} <<\alpha_L \overline{v_{1L}^2}>>$$

Let us introduce the nondimensional quantities

$$p_* = \frac{<<\overline{p}>>}{\rho_L \overline{U}_L^2} \qquad x_* = \frac{2}{\hat{r}} \cdot x_1$$

Then easy but tedious calculations lead from system II under the assumptions II to the final system:

III

$$\frac{d\alpha}{dx_*} = \frac{\alpha(1-\alpha)}{3\alpha^3 + \left(\frac{\overline{U}_G}{\overline{U}_L}\right)^2 \cdot (1-\alpha)^3} \cdot \left[\frac{\overline{U}_G}{\overline{U}_L} \cdot (1-\alpha) - \Gamma\alpha\right]^2$$

$$-\frac{dp_*}{dx_*} = \frac{1}{(1-\alpha)^2} \cdot \frac{d\alpha}{dx_*} + \frac{0.316\hat{r}}{2D_H} \cdot (1-\alpha)^{-1.75} \cdot \left(\frac{\overline{U}_L D_H}{\nu_L}\right)^{-0.25}$$

where $<<\alpha>>$ is written as α.

Manuscript received July 12, 1976; revision received November 29, and accepted December 14, 1976.